Engineering Structures 34 (2012) 414–420

Contents lists available at SciVerse ScienceDirect

Engineering Structures

journal homepage: www.elsevier.com/locate/engstruct

A direct method for analyzing the vertical vehicle–structure interaction

S.G.M. Neves *, A.F.M. Azevedo, R. Calçada

Centro de Estudos da Construção, Faculdade de Engenharia, Universidade do Porto, Rua Dr. Roberto Frias, 4200-465 Porto, Portugal

ARTICLE INFO

Article history:
Received 24 June 2011
Revised 24 September 2011
Accepted 3 October 2011
Available online 10 November 2011

Keywords:
Vehicle–structure interaction
Contact
High-speed train
Bridge
Dynamic analysis

ABSTRACT

A new method for the dynamic analysis of the vertical vehicle–structure interaction is presented. The vehicle and structure systems can be discretized with various types of finite elements and may have any degree of complexity. The equations of both systems are complemented with additional compatibility equations to ensure contact between the vehicles and the structure. The equations of motion and the compatibility equations form a single system that is solved directly, thus avoiding the iterative procedure used by other authors to satisfy the compatibility between the vehicle and structure. For large structural systems the proposed method is usually more efficient than those that frequently update and factorize the system matrix. Some numerical examples have shown that the proposed formulation is accurate and efficient.

1. Introduction

Research on the dynamic analysis of the vehicle–structure interaction is an important issue in civil engineering. A state-of-the-art review on the analysis of the vehicle–structure interaction is briefly presented here. Additional information on this subject can be found in Diana and Cheli [1], Knothe and Grassie [2] and Popp et al. [3].

The dynamic analysis of the vehicle–structure interaction can be performed in the frequency domain or in the time domain. The frequency domain methods require less computational effort but may impose some restrictions when dealing with non-periodic effects and nonlinear structural models [3]. There are several nonlinearities in the vehicle–structure system that should be considered, such as the nonlinear contact, the state-dependent rail pads and ballast/subgrade properties, and the loss of contact between sleepers and ballast [4,5]. In these cases, the time domain methods are more appropriate.

There are several studies that emphasize the importance of considering vertical vehicle–structure interaction. Zhai and Cai [6] concluded that the irregularities on the surfaces of wheel and rail induce severe dynamic disturbances. As a consequence, large impact forces occur, being the principal cause of damage to the wheels, rails and other vehicle and track components. The formation and development of wheel and rail irregularities and the increase of the dynamic interaction forces are interrelated. Yau et al. [7] pointed out that the riding comfort of rail cars moving over simple beams can be considerably affected by the rail irregularity, ballast stiffness, suspension stiffness and suspension damping. Therefore, the design of high-speed railway bridges may be governed by serviceability limit states, such as the riding comfort, rather than by ultimate limit states.

The simulation of the vehicle–structure system requires the coupling of two independent meshes. The dynamic equilibrium is defined by two sets of equations of motion, one for the vehicle and the other for the structure. Both sets of equations can be solved by an iterative procedure to ensure the coupling of the two subsystems [8–10]. These methods may require a considerable computational effort when dealing with a large number of contact points due to a probable slow rate of convergence.

Other approaches for solving the two sets of equations of motion are based on condensation techniques that eliminate the degrees of freedom of the vehicle at the element level. Yang and Yau [11] used the Newmark method to reduce the vehicle equations to equivalent stiffness equations, which are then condensed to those of the bridge elements in contact. The derived element ignores the pitching effect of the vehicle, which may significantly affect its response. Yang et al. [12] presented an improved vehicle–bridge interaction element to overcome this drawback. Yang and Wu [13] developed a procedure capable of simulating vehicles of varying complexity. Since the position of each contact point changes over time, the system matrix used by these methods [11–13] is usually time–dependent and must be updated and factorized at each time step. This procedure may demand a considerable computational effort.

The main objective of this paper is to present an accurate, efficient and simple method for problems in two or three

* Corresponding author. Tel.: +351 22 508 1901; fax: +351 22 508 1446.
E-mail addresses: sgm.neves@fe.up.pt (S.G.M. Neves), alvaro@fe.up.pt (A.F.M. Azevedo), ruiabc@fe.up.pt (R. Calçada).

0141-0296/$ - see front matter © 2011 Elsevier Ltd. All rights reserved.
doi:10.1016/j.engstruct.2011.10.010

Nomenclature

a_0	amplitude of the irregularity function
C	viscous damping matrix
E	Young's modulus
F	load vector
g	acceleration of gravity
I	moment of inertia of the cross section
k_v	spring stiffness
K	stiffness matrix
L	beam length
m	mass per unit length
M	mass matrix
M_n	generalized mass of the nth mode
M_v	suspended mass
P	external load vector
q_n	normal coordinate of the nth mode
r	irregularities between vehicle and structure
R	support reactions
u	displacement vector
v	speed of the vehicle
X	contact forces acting on the vehicle
Y	contact forces acting on the structure
z	absolute displacement of the mass
λ	wavelength of the irregularity function
ν	Poisson's ratio
ξ	sprung mass distance from the left end of the beam
ϕ_n	mode shape of the nth mode
ω_n	natural frequency of the nth mode

Subscripts

F	includes I and X type d.o.f.
I	unconstrained nodal d.o.f.
P	prescribed nodal d.o.f.
X	contact nodal d.o.f. of the vehicle
Y	contact d.o.f. in a non-nodal point of the surface of the structure

Superscripts

c	current time step ($t + \Delta t$)
p	previous time step (t)

dimensions, which is capable of analyzing the vertical dynamic interaction between vehicles and structures, especially at low frequencies. In the developed procedure the subsystems that model the structure and the vehicles may have any degree of complexity and can be discretized with various types of finite elements, such as beams, shells and solids.

The proposed method is used to analyze the contact between nodes of the vehicles and the surface of the structure. At each instant, the equations of motion of the structure and vehicles are complemented with additional compatibility equations that relate nodal displacements of the vehicles to the displacements of the corresponding points on the surface of the structure, with no sliding or separation being allowed. The irregularities at the contact interface can be considered in the compatibility equations. The equations of motion and the compatibility equations form a single system with displacements and contact forces as unknowns. This system is solved directly, thus avoiding the iterative procedure used by other authors to satisfy the compatibility equations [8–10]. The proposed formulation is referred to as the direct method and has been implemented in FEMIX, which is a general purpose finite element computer program [14].

2. Vehicle–structure interaction

A general vehicle model moving at speed $v(t)$ over a simple structure is represented in Fig. 1. The vehicle and structure subsystems can be modeled with various types of finite elements, such as beams, shells and solids.

Fig. 1 shows the contact forces acting on the vehicle (X_i), the contact forces acting on the structure (Y_i) and the irregularities between the contact points of the vehicle and the structure (r_i). The degrees of freedom (d.o.f.) are grouped according to the classification presented in Table 1.

2.1. Formulation of the equations of motion

Based on the α method [15], the equations of motion of the vehicle–structure system can be expressed as

$$\mathbf{M}\,\ddot{\mathbf{u}}^c + (1+\alpha)\,\mathbf{C}\,\dot{\mathbf{u}}^c - \alpha\,\mathbf{C}\,\dot{\mathbf{u}}^p + (1+\alpha)\,\mathbf{K}\,\mathbf{u}^c - \alpha\,\mathbf{K}\,\mathbf{u}^p = (1+\alpha)\,\mathbf{F}^{\,c} - \alpha\,\mathbf{F}^p \tag{1}$$

where **M** is the mass matrix, **C** is the viscous damping matrix, **K** is the stiffness matrix, **F** is the load vector, **u** are the displacements and α is the parameter of the α method. Adopting $\alpha = 0$, this algorithm reduces to the Newmark method and, for other values, numerical dissipation is introduced in the higher modes. The superscript c indicates the current time step ($t + \Delta t$) and the superscript p indicates the previous one (t).

According to the adopted d.o.f. classification (see Table 1), the matrices and vectors of Eq. (1) are partitioned into the form

$$\begin{bmatrix}\mathbf{M}_{FF} & \mathbf{M}_{FP}\\ \mathbf{M}_{PF} & \mathbf{M}_{PP}\end{bmatrix}\begin{bmatrix}\ddot{\mathbf{u}}_F^c\\ \ddot{\mathbf{u}}_P^c\end{bmatrix} + (1+\alpha)\begin{bmatrix}\mathbf{C}_{FF} & \mathbf{C}_{FP}\\ \mathbf{C}_{PF} & \mathbf{C}_{PP}\end{bmatrix}\begin{bmatrix}\dot{\mathbf{u}}_F^c\\ \dot{\mathbf{u}}_P^c\end{bmatrix} - \alpha\begin{bmatrix}\mathbf{C}_{FF} & \mathbf{C}_{FP}\\ \mathbf{C}_{PF} & \mathbf{C}_{PP}\end{bmatrix}\begin{bmatrix}\dot{\mathbf{u}}_F^p\\ \dot{\mathbf{u}}_P^p\end{bmatrix}$$
$$+ (1+\alpha)\begin{bmatrix}\mathbf{K}_{FF} & \mathbf{K}_{FP}\\ \mathbf{K}_{PF} & \mathbf{K}_{PP}\end{bmatrix}\begin{bmatrix}\mathbf{u}_F^c\\ \mathbf{u}_P^c\end{bmatrix} - \alpha\begin{bmatrix}\mathbf{K}_{FF} & \mathbf{K}_{FP}\\ \mathbf{K}_{PF} & \mathbf{K}_{PP}\end{bmatrix}\begin{bmatrix}\mathbf{u}_F^p\\ \mathbf{u}_P^p\end{bmatrix}$$
$$= (1+\alpha)\begin{bmatrix}\mathbf{F}_F^c\\ \mathbf{F}_P^c\end{bmatrix} - \alpha\begin{bmatrix}\mathbf{F}_F^p\\ \mathbf{F}_P^p\end{bmatrix} \tag{2}$$

In the present paper, the implementation of the contact between nodes of the vehicles and points on the surface of the structure is described. Each Y type d.o.f. corresponds to a d.o.f. at

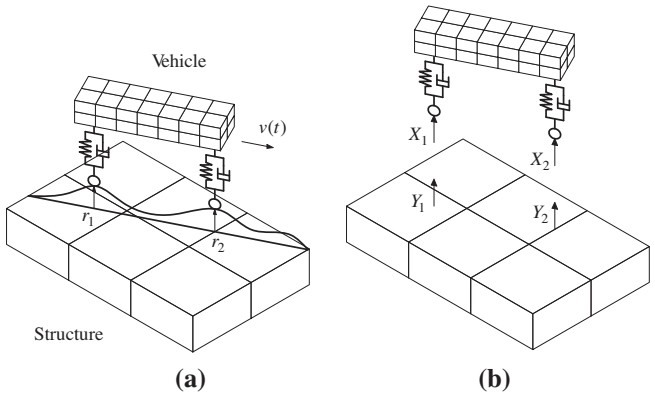

Fig. 1. Vehicle–structure system: (a) schematic illustration and (b) free body diagram.

Table 1
Classification of the degrees of freedom (d.o.f.).

I	Unconstrained nodal d.o.f. (n_I = number of *I* type d.o.f.)
X	Contact nodal d.o.f. of the vehicle (n_X = number of *X* type d.o.f.)
F	Includes *I* and *X* type d.o.f. ($n_F = n_I + n_X$)
Y	Contact d.o.f. in a non-nodal point of the surface of the structure ($n_Y = n_X$)
P	Prescribed nodal d.o.f. (n_P = number of *P* type d.o.f.)

a point located on the surface of the structure and is not associated with any node. For this reason, this type of d.o.f. is not included in Eq. (2).

According to the adopted d.o.f. classification (see Table 1), the load vector can be expressed as

$$\mathbf{F}_I = \mathbf{P}_I + \mathbf{D}_{IY}\,\mathbf{Y}_Y \tag{3}$$

$$\mathbf{F}_X = \mathbf{P}_X + \mathbf{I}_{XX}\,\mathbf{X}_X \tag{4}$$

$$\mathbf{F}_P = \mathbf{P}_P + \mathbf{D}_{PY}\,\mathbf{Y}_Y + \mathbf{R}_P \tag{5}$$

where $\mathbf{P}_I$, $\mathbf{P}_X$ and $\mathbf{P}_P$ are the external load vectors, $\mathbf{R}_P$ are the support reactions, and $\mathbf{I}_{XX}$ is the identity matrix. Each element D_{ij} of the matrices $\mathbf{D}_{IY}$ and $\mathbf{D}_{PY}$ corresponds to the equivalent nodal load in d.o.f. *i* due to a unit load applied in d.o.f. *j*. The *X* type d.o.f. are located in nodal points of the vehicle and the *Y* type d.o.f. are located in non-nodal points of the surface of the structure (see Fig. 1).

According to Fig. 1,

$$\mathbf{X}_X + \mathbf{Y}_Y = 0 \tag{6}$$

being the number of *Y* type d.o.f. equal to the number of *X* type d.o.f. Substituting Eq. (6) into Eqs. (3) and (5) and replacing the subscript *Y* with *X* yields

$$\mathbf{F}_I = \mathbf{P}_I - \mathbf{D}_{IX}\,\mathbf{X}_X \tag{7}$$

$$\mathbf{F}_P = \mathbf{P}_P - \mathbf{D}_{PX}\,\mathbf{X}_X + \mathbf{R}_P \tag{8}$$

Eqs. (4) and (7) can be written in the form

$$\mathbf{F}_F = \mathbf{P}_F + \mathbf{G}_{FX}\,\mathbf{X}_X \tag{9}$$

where

$$\mathbf{F}_F = \begin{bmatrix}\mathbf{F}_I\\ \mathbf{F}_X\end{bmatrix} \qquad \mathbf{P}_F = \begin{bmatrix}\mathbf{P}_I\\ \mathbf{P}_X\end{bmatrix} \tag{10}$$

and

$$\mathbf{G}_{FX} = \begin{bmatrix}-\mathbf{D}_{IX}\\ \mathbf{I}_{XX}\end{bmatrix} \tag{11}$$

Substituting Eqs. (8) and (9) into Eq. (2), and rearranging, the following equations are obtained

$$\begin{aligned}\mathbf{M}_{FF}\,\ddot{\mathbf{u}}_F^c + (1+\alpha)\,\mathbf{C}_{FF}\,\dot{\mathbf{u}}_F^c + (1+\alpha)\,\mathbf{K}_{FF}\,\mathbf{u}_F^c - (1+\alpha)\,\mathbf{G}_{FX}\,\mathbf{X}_X^c = (1+\alpha)\,\mathbf{P}_F^c - \alpha\,\mathbf{P}_F^p\\ -\alpha\,\mathbf{G}_{FX}\,\mathbf{X}_X^p - \mathbf{M}_{FP}\,\ddot{\mathbf{u}}_P^c - (1+\alpha)\,\mathbf{C}_{FP}\,\dot{\mathbf{u}}_P^c + \alpha\,\mathbf{C}_{FF}\,\dot{\mathbf{u}}_F^p + \alpha\,\mathbf{C}_{FP}\,\dot{\mathbf{u}}_P^p - (1+\alpha)\,\mathbf{K}_{FP}\,\mathbf{u}_P^c\\ +\alpha\,\mathbf{K}_{FF}\,\mathbf{u}_F^p + \alpha\,\mathbf{K}_{FP}\,\mathbf{u}_P^p\end{aligned} \tag{12}$$

$$\begin{aligned}\mathbf{R}_P^c = \tfrac{\alpha}{1+\alpha}\,\mathbf{R}_P^p - \mathbf{P}_P^c + \tfrac{\alpha}{1+\alpha}\,\mathbf{P}_P^p + \mathbf{D}_{PX}\,\mathbf{X}_X^c - \tfrac{\alpha}{1+\alpha}\,\mathbf{D}_{PX}\,\mathbf{X}_X^p + \tfrac{1}{1+\alpha}\,\mathbf{M}_{PF}\,\ddot{\mathbf{u}}_F^c + \tfrac{1}{1+\alpha}\,\mathbf{M}_{PP}\,\ddot{\mathbf{u}}_P^c\\ +\mathbf{C}_{PF}\,\dot{\mathbf{u}}_F^c + \mathbf{C}_{PP}\,\dot{\mathbf{u}}_P^c - \tfrac{\alpha}{1+\alpha}\,\mathbf{C}_{PF}\,\dot{\mathbf{u}}_F^p - \tfrac{\alpha}{1+\alpha}\,\mathbf{C}_{PP}\,\dot{\mathbf{u}}_P^p + \mathbf{K}_{PF}\,\mathbf{u}_F^c + \mathbf{K}_{PP}\,\mathbf{u}_P^c - \tfrac{\alpha}{1+\alpha}\,\mathbf{K}_{PF}\,\mathbf{u}_F^p\\ -\tfrac{\alpha}{1+\alpha}\,\mathbf{K}_{PP}\,\mathbf{u}_P^p\end{aligned} \tag{13}$$

The support reactions $\mathbf{R}_P^c$ given by Eq. (13) can be calculated after solving the system of linear equations defined by Eq. (12)

Eq. (12) can be written in the form

$$\mathbf{M}_{FF}\,\ddot{\mathbf{u}}_F^c + (1+\alpha)\,\mathbf{C}_{FF}\,\dot{\mathbf{u}}_F^c + (1+\alpha)\,\mathbf{K}_{FF}\,\mathbf{u}_F^c - (1+\alpha)\,\mathbf{G}_{FX}\,\mathbf{X}_X^c = \bar{\bar{\mathbf{F}}}_F \tag{14}$$

where

$$\begin{aligned}\bar{\bar{\mathbf{F}}}_F = (1+\alpha)\,\mathbf{P}_F^c - \alpha\,\mathbf{P}_F^p - \alpha\,\mathbf{G}_{FX}\,\mathbf{X}_X^p - \mathbf{M}_{FP}\,\ddot{\mathbf{u}}_P^c - (1+\alpha)\,\mathbf{C}_{FP}\,\dot{\mathbf{u}}_P^c + \alpha\,\mathbf{C}_{FF}\,\dot{\mathbf{u}}_F^p + \alpha\,\mathbf{C}_{FP}\,\dot{\mathbf{u}}_P^p\\ -(1+\alpha)\,\mathbf{K}_{FP}\,\mathbf{u}_P^c + \alpha\,\mathbf{K}_{FF}\,\mathbf{u}_F^p + \alpha\,\mathbf{K}_{FP}\,\mathbf{u}_P^p\end{aligned} \tag{15}$$

In the Newmark method [16] the velocity and displacement at the current time step ($t + \Delta t$) are approximated with

$$\dot{\mathbf{u}}_F^c = \dot{\mathbf{u}}_F^p + \left[(1-\gamma)\,\ddot{\mathbf{u}}_F^p + \gamma\,\ddot{\mathbf{u}}_F^c\right]\Delta t \tag{16}$$

$$\mathbf{u}_F^c = \mathbf{u}_F^p + \dot{\mathbf{u}}_F^p\,\Delta t + \left[\left(\frac{1}{2}-\beta\right)\ddot{\mathbf{u}}_F^p + \beta\,\ddot{\mathbf{u}}_F^c\right]\Delta t^2 \tag{17}$$

These equations are also valid for the α method. The parameters γ and β influence the stability and accuracy of the Newmark and α methods. Solving Eq. (17) for $\ddot{\mathbf{u}}_F^c$ gives

$$\ddot{\mathbf{u}}_F^c = \frac{1}{\beta\Delta t^2}\,\mathbf{u}_F^c - \frac{1}{\beta\Delta t^2}\,\mathbf{u}_F^p - \frac{1}{\beta\Delta t}\,\dot{\mathbf{u}}_F^p - \left(\frac{1}{2\beta}-1\right)\ddot{\mathbf{u}}_F^p \tag{18}$$

Substituting $\ddot{\mathbf{u}}_F^c$ given by Eq. (18) into Eq. (16) yields

$$\begin{aligned}\dot{\mathbf{u}}_F^c = \dot{\mathbf{u}}_F^p + (1-\gamma)\,\Delta t\,\ddot{\mathbf{u}}_F^p\\ +\gamma\,\Delta t\left[\frac{1}{\beta\Delta t^2}\,\mathbf{u}_F^c - \frac{1}{\beta\Delta t^2}\,\mathbf{u}_F^p - \frac{1}{\beta\Delta t}\,\dot{\mathbf{u}}_F^p - \left(\frac{1}{2\beta}-1\right)\ddot{\mathbf{u}}_F^p\right]\end{aligned} \tag{19}$$

This equation can be written in the form

$$\dot{\mathbf{u}}_F^c = \frac{\gamma}{\beta\Delta t}\,\mathbf{u}_F^c - \frac{\gamma}{\beta\Delta t}\,\mathbf{u}_F^p + \left(1-\frac{\gamma}{\beta}\right)\dot{\mathbf{u}}_F^p + \Delta t\left(1-\frac{\gamma}{2\beta}\right)\ddot{\mathbf{u}}_F^p \tag{20}$$

Substituting Eqs. (18) and (20) into Eq. (14), and rearranging the terms, yields

$$\bar{\mathbf{K}}_{FF}\,\mathbf{u}_F^c - (1+\alpha)\,\mathbf{G}_{FX}\,\mathbf{X}_X^c = \bar{\bar{\mathbf{F}}}_F \tag{21}$$

where

$$\bar{\mathbf{K}}_{FF} = A_0\,\mathbf{M}_{FF} + (1+\alpha)\,A_1\,\mathbf{C}_{FF} + (1+\alpha)\,\mathbf{K}_{FF} \tag{22}$$

$$\begin{aligned}\bar{\bar{\mathbf{F}}}_F = \bar{\mathbf{F}}_F + \mathbf{M}_{FF}\left[A_0\,\mathbf{u}_F^p + A_2\,\dot{\mathbf{u}}_F^p + A_3\,\ddot{\mathbf{u}}_F^p\right]\\ +(1+\alpha)\,\mathbf{C}_{FF}\left[A_1\,\mathbf{u}_F^p + A_4\,\dot{\mathbf{u}}_F^p + A_5\,\ddot{\mathbf{u}}_F^p\right]\end{aligned} \tag{23}$$

$$A_0 = \frac{1}{\beta\Delta t^2} \qquad A_1 = \frac{\gamma}{\beta\Delta t} \qquad A_2 = \frac{1}{\beta\Delta t}$$

$$A_3 = \frac{1}{2\beta} - 1 \qquad A_4 = \frac{\gamma}{\beta} - 1 \qquad A_5 = \Delta t\left(\frac{\gamma}{2\beta} - 1\right) \tag{24}$$

In matrix notation, Eq. (21) may be expressed as

$$\begin{bmatrix}\bar{\mathbf{K}}_{FF} & \bar{\mathbf{G}}_{FX}\end{bmatrix}\begin{bmatrix}\mathbf{u}_F^c\\ \mathbf{X}_X^c\end{bmatrix} = \begin{bmatrix}\bar{\bar{\mathbf{F}}}_F\end{bmatrix} \tag{25}$$

where

$$\bar{\mathbf{G}}_{FX} = -(1+\alpha)\,\mathbf{G}_{FX} \tag{26}$$

2.2. Formulation of the compatibility equations

At each instant, the equations of motion of the structure and vehicles are complemented with additional compatibility equations to ensure the contact between the nodes of the vehicles and the surface of the structure. The subtraction between a displacement of a node of the vehicle and the corresponding displacement of the surface of the structure must be equal to the irregularity at the contact interface, with no sliding or separation being allowed (see Fig. 1). The compatibility equations for the current time step ($t + \Delta t$) can be expressed as

$$\mathbf{u}_X^c - \mathbf{u}_Y^c = \mathbf{r}_X^c \tag{27}$$

where

$$\mathbf{u}_Y^c = \mathbf{E}_{YI}\,\mathbf{u}_I^c + \mathbf{E}_{YP}\,\mathbf{u}_P^c \tag{28}$$

In this equation each element E_{ij} of the matrices $\mathbf{E}_{YI}$ and $\mathbf{E}_{YP}$ corresponds to the displacement at an internal d.o.f. i due to a unit displacement at nodal d.o.f. j. Since the number of Y type d.o.f. is equal to the number of X type d.o.f., in Eq. (28) the subscript Y is replaced with the subscript X, yielding

$$\mathbf{u}_Y^c = \mathbf{E}_{XI}\,\mathbf{u}_I^c + \mathbf{E}_{XP}\,\mathbf{u}_P^c \tag{29}$$

Substituting Eq. (29) into Eq. (27) and rearranging leads to

$$-\mathbf{E}_{XI}\,\mathbf{u}_I^c + \mathbf{u}_X^c = \mathbf{r}_X^c + \mathbf{E}_{XP}\,\mathbf{u}_P^c \tag{30}$$

According to the adopted classification of d.o.f. (see Table 1), Eq. (30) can be written in the form

$$\mathbf{H}_{XF}\,\mathbf{u}_F^c = \mathbf{r}_X^c + \mathbf{E}_{XP}\,\mathbf{u}_P^c \tag{31}$$

where

$$\mathbf{u}_F = \begin{bmatrix} \mathbf{u}_I \\ \mathbf{u}_X \end{bmatrix} \tag{32}$$

and

$$\mathbf{H}_{XF} = [\,-\mathbf{E}_{XI} \quad \mathbf{I}_{XX}\,] \tag{33}$$

Premultiplying Eq. (31) by $-(1+\alpha)$ gives

$$-(1+\alpha)\,\mathbf{H}_{XF}\,\mathbf{u}_F^c = -(1+\alpha)\,\mathbf{r}_X^c - (1+\alpha)\,\mathbf{E}_{XP}\,\mathbf{u}_P^c \tag{34}$$

2.3. Complete system of equations

Eqs. (25) and (34) can be expressed in matrix form leading to the following complete system of linear equations

$$\begin{bmatrix} \bar{\mathbf{K}}_{FF} & \bar{\mathbf{G}}_{FX} \\ \bar{\mathbf{H}}_{XF} & \mathbf{0} \end{bmatrix} \begin{bmatrix} \mathbf{u}_F^c \\ \mathbf{X}_X^c \end{bmatrix} = \begin{bmatrix} \bar{\mathbf{F}}_F \\ \bar{\mathbf{r}}_X \end{bmatrix} \tag{35}$$

in which

$$\bar{\mathbf{H}}_{XF} = -(1+\alpha)\,\mathbf{H}_{XF} \tag{36}$$

$$\bar{\mathbf{r}}_X = -(1+\alpha)\,\mathbf{r}_X^c - (1+\alpha)\,\mathbf{E}_{XP}\,\mathbf{u}_P^c \tag{37}$$

The symmetry of the coefficient matrix (35) can be demonstrated using the Betti's theorem.

Since the time required to solve the system of linear equations (35) may represent a large percentage of the total solution time [17], the efficiency of the solver is very important. The present method uses an efficient and stable block factorization algorithm (see Appendix A) that takes into account the specific properties of each block, namely, symmetry, positive definiteness and bandwidth.

In Eq. (35) the coefficient matrix is composed of the stiffness matrix $\bar{\mathbf{K}}_{FF}$ and three additional blocks $\bar{\mathbf{G}}_{FX}$, $\bar{\mathbf{H}}_{XF}$ and $\mathbf{0}$. When compared with other procedures [11–13], the solution of the system requires the additional matrix operations (A.5), (A.6), (A.7), (A.11), (A.12) and part of (A.13) (see Appendix A). For large structural systems, where n_F and n_X are usually of the order of tens of thousands and tens, respectively, of all the additional operations only the time required by (A.5) is significant when compared with the total solution time.

In general, the effective stiffness matrix $\bar{\mathbf{K}}_{FF}$ remains constant during a linear analysis or has to be updated and factorized only at certain times during a nonlinear analysis. Since in the direct method only the additional blocks of the coefficient matrix (35) are modified, further factorizations (A.4) are avoided. Since, for large structural systems, the additional forward substitutions (A.5) require less computational effort than the additional factorizations (A.4), the direct method can be considerably more efficient than those that need to factorize the stiffness matrix at every time step [11–13].

3. Numerical examples and verification

In this section, two numerical examples are used to verify the accuracy and efficiency of the direct method and the associated computer program. The first example consists of a simply supported beam subjected to a single moving sprung mass and the second consists of the same beam subjected to 50 moving sprung masses. In both examples, the results obtained with the direct method are compared with semi-analytical solutions.

3.1. Simply supported beam subjected to one moving sprung mass

A simply supported beam subjected to a moving sprung mass is illustrated in Fig. 2, where ξ is the sprung mass distance from the left end and z is the absolute displacement of the mass. The properties of the system correspond to those adopted by Yang and Yau [11], being the beam length $L = 25.0$ m and the geometrical and mechanical properties the following: Young's modulus $E = 2.87$ GPa, Poisson's ratio $\nu = 0.2$, moment of inertia $I = 2.90\ \text{m}^4$, mass per unit length $m = 2303\ \text{kg m}^{-1}$, suspended mass $M_v = 5750$ kg and spring stiffness $k_v = 1595\ \text{kN m}^{-1}$. The first natural frequency of the beam is $\omega_1 = 30.02\ \text{rad s}^{-1}$, the natural frequency of the spring-mass system is $\omega_v = 16.66\ \text{rad s}^{-1}$ and the mass ratio is $M_v/(mL) = 0.1$. The sprung mass moves at a constant speed $v = 100\ \text{km h}^{-1}$.

By neglecting the damping effect, the shear deformation and the rotary inertia, the nth modal equation of motion governing the transverse vibration of a simply supported beam can be expressed as [18]

$$\ddot{q}_n(t) + \omega_n^2 q_n(t) + \frac{\delta k_v \phi_n(\xi) \sum_{m=1}^{\infty} \phi_m(\xi)\, q_m(t)}{M_n} - \frac{\delta k_v \phi_n(\xi) z}{M_n} = \frac{\delta M_v g \phi_n(\xi)}{M_n} \tag{38}$$

In this equation $q_n(t)$ is the normal coordinate of the nth mode, being ω_n the natural frequency, ϕ_n the mode shape and M_n the generalized mass. The parameter δ assumes the value one if $0 \leqslant \xi \leqslant L$, and zero otherwise (see Fig. 2), and g is the acceleration of gravity. Since z is measured from the neutral spring position, the term $M_v\,g$ must be included.

The governing equation of motion of the sprung mass is given by

$$M_v\,\ddot{z} + k_v \left[z - \sum_{m=1}^{\infty} \phi_m(\xi)\, q_m(t) \right] = 0 \tag{39}$$

The computer program FEMIX 4.0 [14] was used to perform the dynamic finite element analysis. The following parameters for the α method are considered: $\Delta t = 0.001$ s, $\beta = 0.25$, $\gamma = 0.5$ and $\alpha = 0$. The structure is discretized with 50 beam elements and the total number of time steps is 900. The semi-analytical solution of Eqs.

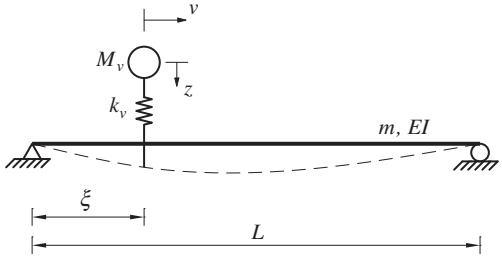

Fig. 2. Simply supported beam subjected to a moving sprung mass.

(38) and (39) is obtained considering the contribution of the first twenty modes of vibration, using the same integration method and parameters.

The semi-analytical solutions for the vertical displacement and acceleration at the midpoint of the beam and the corresponding finite element approximations based on the direct method are plotted in Figs. 3 and 4.

The dynamic responses of the sprung mass, in terms of vertical displacement and acceleration, are shown in Figs. 5 and 6.

The results obtained with the proposed formulation perfectly match the corresponding semi-analytical solutions. The comparison between the results obtained and those published by Yang and Yau [11] shows that the present inclusion of additional modes of vibration leads to a better agreement, especially for the case of the sprung mass response.

3.2. Simply supported beam subjected to 50 moving sprung masses

The beam described in Section 3.1 is now subjected to 50 sprung masses moving at a constant speed $v = 47.7$ km h^{-1}. The distance between masses is 3.0 m, being M_v and k_v unaltered. A simple sinusoidal function defined by Eq. (40) is considered for the validation of the effects of irregularities at the contact interface.

$$r(\xi) = a_0 \sin\left(\frac{2\pi\xi}{\lambda}\right) \tag{40}$$

In Eq. (40), a_0 is the amplitude (0.5 mm) and λ is the wavelength (5.0 m) of the irregularity. The wavelength chosen is one fifth of the span length. The speed of the sprung masses and the wavelength of the irregularity are such that the frequency of excitation is equal to the natural frequency of the spring-mass system.

For the case of several moving sprung masses, Eqs. (38) and (39) become

$$\ddot{q}_n(t) + {\omega_n}^2 q_n(t) + \sum_{i=1}^{N_v} \frac{\delta_i k_{vi} \phi_n(\xi_i) \sum_{m=1}^{\infty} \phi_m(\xi_i) q_m(t)}{M_n} - \sum_{i=1}^{N_v} \frac{\delta_i k_{vi} \phi_n(\xi_i) z_i}{M_n} = \sum_{i=1}^{N_v} \frac{\delta_i (M_{vi} g - k_{vi} r_i) \phi_n(\xi_i)}{M_n} \tag{41}$$

$$M_{vi} \ddot{z}_i + k_{vi} \left[z_i - r_i - \sum_{m=1}^{\infty} \phi_m(\xi_i)\, q_m(t) \right] = 0 \tag{42}$$

being N_v the number of sprung masses.

The parameters used in the dynamic finite element analysis and in the semi-analytical solution of Eqs. (41) and (42) are the same as those used in the previous example. The total number of time steps is now 14000.

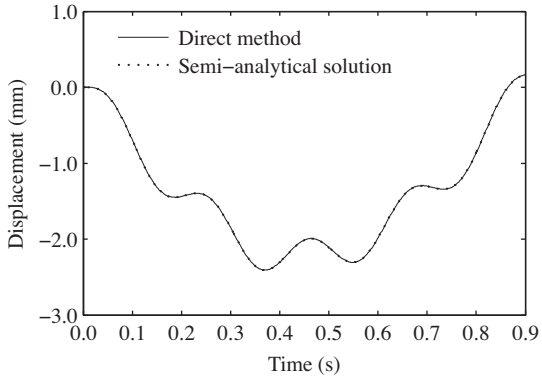

Fig. 3. Vertical displacement at the midpoint of the beam.

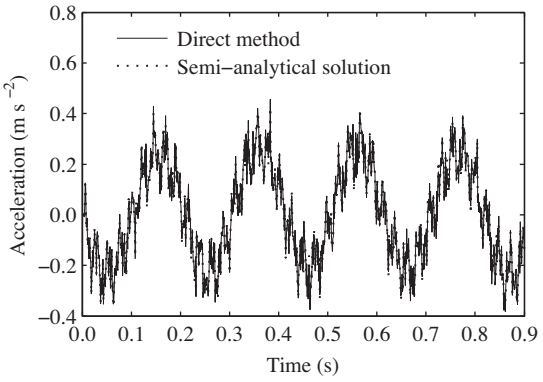

Fig. 4. Vertical acceleration at the midpoint of the beam.

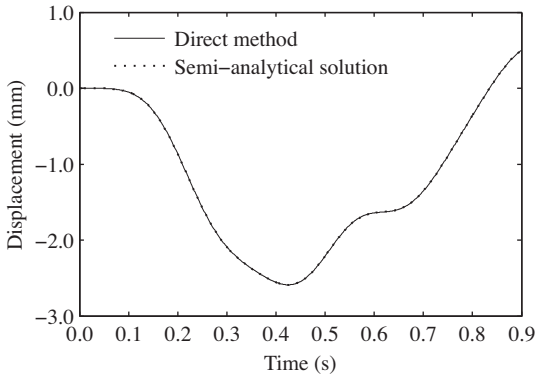

Fig. 5. Vertical displacement of the sprung mass.

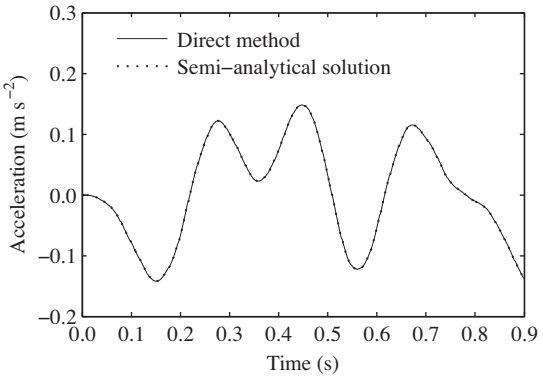

Fig. 6. Vertical acceleration of the sprung mass.

The semi-analytical solutions for the vertical displacement and acceleration of the first sprung mass over the time interval [0,3] (s) and the corresponding finite element approximations based on the direct method are plotted in Figs. 7 and 8.

The vertical displacement and acceleration of the last sprung mass over the time interval [11,14](s) are shown in Figs. 9 and 10.

The results obtained with the direct method show a very good agreement with the corresponding semi-analytical solutions.

In order to test the efficiency of the direct method, the beam analyzed in this section is now discretized with 10000 8-node solid elements ($10 \times 10 \times 100$) and has 36597 unconstrained d.o.f. This beam has a rectangular cross section of width $b = 2.2272$ m and height $h = 2.5$ m (see Fig. 11). The parameters used in the previous analysis remain unchanged.

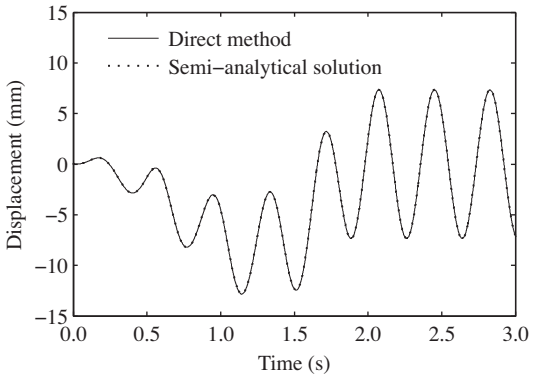

Fig. 7. Vertical displacement of the first sprung mass.

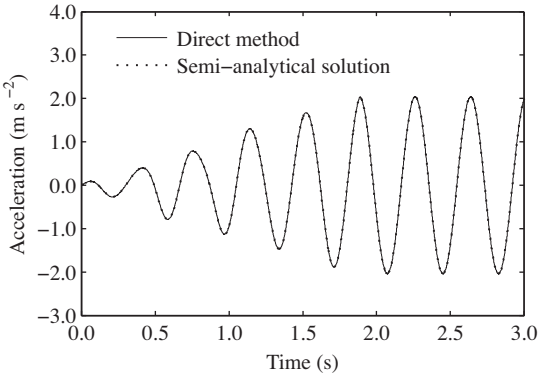

Fig. 8. Vertical acceleration of the first sprung mass.

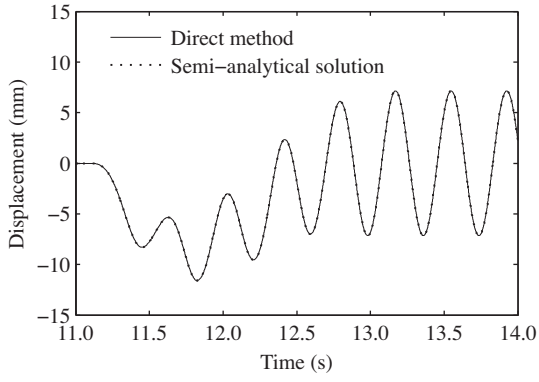

Fig. 9. Vertical displacement of the last sprung mass.

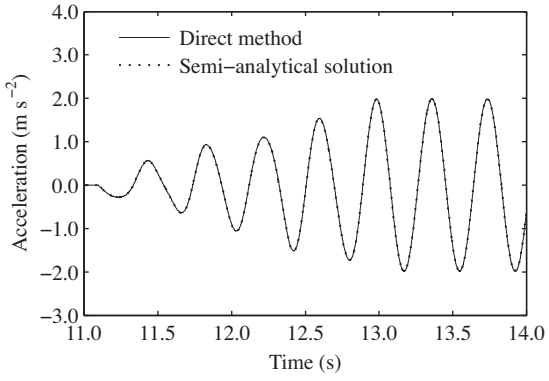

Fig. 10. Vertical acceleration of the last sprung mass.

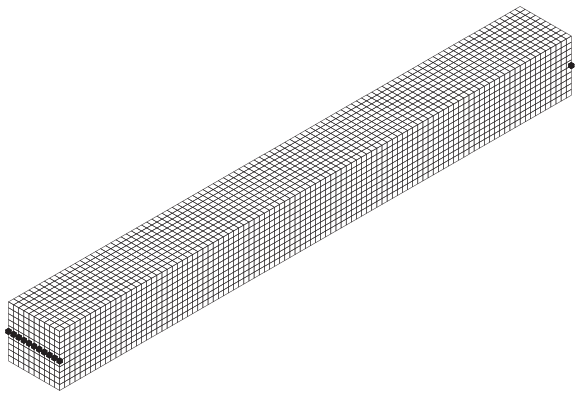

Fig. 11. Simply supported beam modeled with three-dimensional solid elements.

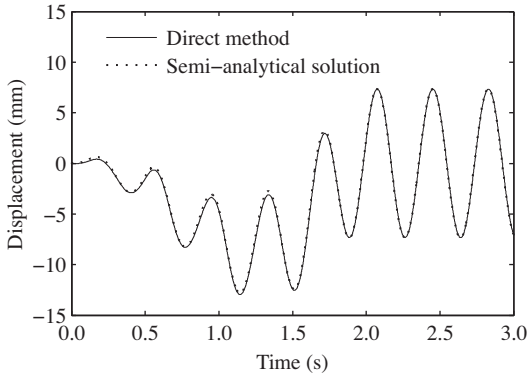

Fig. 12. Vertical displacement of the first sprung mass.

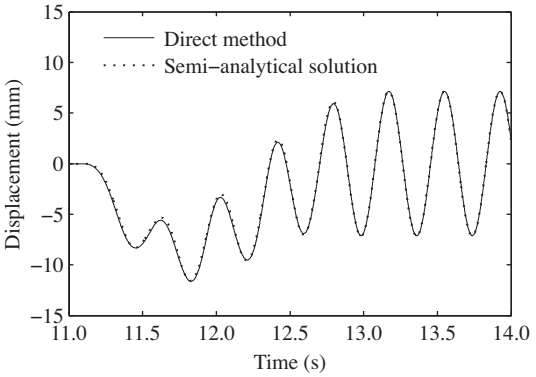

Fig. 13. Vertical displacement of the last sprung mass.

The vertical displacement of the first sprung mass over the time interval [0,3] (s) is shown in Fig. 12.

The vertical displacement of the last sprung mass over the time interval [11,14](s) is plotted in Fig. 13.

The results obtained with the proposed method show a good agreement with the corresponding semi-analytical solution. The slight differences are due to the fact that the semi-analytical solution neglects the shear deformation and rotary inertia whereas the finite element model accounts for such effects.

A workstation with an Intel Core i7-860 processor running at 2.80 GHz was used to perform the calculations. Using a single core, the execution time is 10572 s. According to the authors' experience this result is very satisfactory.

5. Conclusions

An accurate, efficient and simple method for analyzing the vertical interaction between vehicles and structure has been developed. The vehicles and structures can be discretized with complex meshes composed of various types of finite elements.

The equations of motion of the vehicles and structure are combined into a single system that is solved directly, thus avoiding the iterative procedure used by other methods to satisfy the compatibility of displacements. Generally, iterative methods are less accurate and may even diverge. For the case of large structural systems the proposed method is usually more efficient than those that need to frequently update and factorize the system matrix. The implementation of the direct method in a finite element computer program is straightforward for the reason that only the contact algorithm needs to be implemented and no additional finite elements have to be developed.

The accuracy and efficiency of the direct method has been confirmed using two numerical examples. An excellent agreement between the results obtained with the proposed method and the corresponding semi-analytical solutions is observed.

The step-by-step integration procedure presented in this paper can be generalized to the case of a nonlinear analysis by modifying the equation of motion into an incremental form.

Acknowledgements

The authors wish to thank Professor Ana Maria Faustino of the University of Porto for the helpful discussions during the preparation of this manuscript. This paper reports research developed under financial support provided by "FCT – Fundação para a Ciência e Tecnologia", Portugal, under Grant No. SFRH/BD/39190/2007 and Research Project No. PTDC/ECM/69697/2006.

Appendix A. Block factorization

The block factorization of the system of linear equations (35) is presented below using the following notation

$$\begin{bmatrix} \mathbf{A}_{11} & \mathbf{A}_{21}^T \\ \mathbf{A}_{21} & \mathbf{0} \end{bmatrix} \begin{bmatrix} \mathbf{x}_1 \\ \mathbf{x}_2 \end{bmatrix} = \begin{bmatrix} \mathbf{b}_1 \\ \mathbf{b}_2 \end{bmatrix} \tag{A.1}$$

and

$$\mathbf{A} = \begin{bmatrix} \mathbf{A}_{11} & \mathbf{A}_{21}^T \\ \mathbf{A}_{21} & \mathbf{0} \end{bmatrix} \tag{A.2}$$

It is assumed that $\mathbf{A}_{11}$ is a symmetric and positive definite submatrix and $\mathbf{A}_{21}^T$ has full rank. With these assumptions matrix $\mathbf{A}$ admits the following $\mathbf{LDL}^T$ factorization without pivoting [19].

$$\begin{bmatrix} \mathbf{A}_{11} & \mathbf{A}_{21}^T \\ \mathbf{A}_{21} & \mathbf{0} \end{bmatrix} = \begin{bmatrix} \mathbf{L}_{11} & \mathbf{0} \\ \mathbf{L}_{21} & \mathbf{L}_{22} \end{bmatrix} \begin{bmatrix} \mathbf{D}_{11} & \mathbf{0} \\ \mathbf{0} & \mathbf{D}_{22} \end{bmatrix} \begin{bmatrix} \mathbf{L}_{11}^T & \mathbf{L}_{21}^T \\ \mathbf{0} & \mathbf{L}_{22}^T \end{bmatrix} \tag{A.3}$$

where $\mathbf{L}_{11}$ and $\mathbf{L}_{22}$ are unit lower triangular submatrices, $\mathbf{D}_{11}$ is a positive definite diagonal submatrix, and $\mathbf{D}_{22}$ is a negative definite diagonal submatrix. By equating the corresponding blocks in Eq. (A.3) the following relations are obtained

$$\mathbf{A}_{11} = \mathbf{L}_{11}\,\mathbf{D}_{11}\,\mathbf{L}_{11}^T \tag{A.4}$$

$$\mathbf{A}_{21} = \mathbf{L}_{21}\,\mathbf{D}_{11}\,\mathbf{L}_{11}^T \tag{A.5}$$

$$\bar{\mathbf{A}}_{22} = \mathbf{L}_{22}\,\mathbf{D}_{22}\,\mathbf{L}_{22}^T \tag{A.6}$$

where

$$\bar{\mathbf{A}}_{22} = -\mathbf{L}_{21}\,\mathbf{D}_{11}\,\mathbf{L}_{21}^T \tag{A.7}$$

Therefore, the components of the right hand side of Eq. (A.3) can be obtained by factorization of $\mathbf{A}_{11}$, formation of $\mathbf{L}_{21}$ by forward substitution and factorization of $\bar{\mathbf{A}}_{22}$.

The solution of the system of linear equations can be obtained by the following two steps

$$\begin{bmatrix} \mathbf{L}_{11} & \mathbf{0} \\ \mathbf{L}_{21} & \mathbf{L}_{22} \end{bmatrix} \begin{bmatrix} \mathbf{y}_1 \\ \mathbf{y}_2 \end{bmatrix} = \begin{bmatrix} \mathbf{b}_1 \\ \mathbf{b}_2 \end{bmatrix} \tag{A.8}$$

$$\begin{bmatrix} \mathbf{L}_{11}^T & \mathbf{L}_{21}^T \\ \mathbf{0} & \mathbf{L}_{22}^T \end{bmatrix} \begin{bmatrix} \mathbf{x}_1 \\ \mathbf{x}_2 \end{bmatrix} = \begin{bmatrix} \mathbf{D}_{11}^{-1} & \mathbf{0} \\ \mathbf{0} & \mathbf{D}_{22}^{-1} \end{bmatrix} \begin{bmatrix} \mathbf{y}_1 \\ \mathbf{y}_2 \end{bmatrix} \tag{A.9}$$

The vectors $\mathbf{y}_1$ and $\mathbf{y}_2$ are obtained by forward substitution

$$\mathbf{L}_{11}\,\mathbf{y}_1 = \mathbf{b}_1 \tag{A.10}$$

$$\mathbf{L}_{22}\,\mathbf{y}_2 = \mathbf{b}_2 - \mathbf{L}_{21}\,\mathbf{y}_1 \tag{A.11}$$

and the solution of the system ($\mathbf{x}_1$ and $\mathbf{x}_2$) is obtained by back-substitution

$$\mathbf{L}_{22}^T\,\mathbf{x}_2 = \mathbf{D}_{22}^{-1}\,\mathbf{y}_2 \tag{A.12}$$

$$\mathbf{L}_{11}^T\,\mathbf{x}_1 = \mathbf{D}_{11}^{-1}\,\mathbf{y}_1 - \mathbf{L}_{21}^T\mathbf{x}_2 \tag{A.13}$$

References

[1] Diana G, Cheli F. Dynamic interaction of railway systems with large bridges. Vehicle Syst Dyn 1989;18:71–106. doi:10.1080/00423118908968915.
[2] Knothe KL, Grassie SL. Modelling of railway track and vehicle/track interaction at high frequencies. Vehicle Syst Dyn 1993;22:209–62. doi:10.1080/00423119308969027.
[3] Popp K, Kruse H, Kaiser I. Vehicle–track dynamics in the mid-frequency range. Vehicle Syst Dyn 1999;31:423–64. doi:10.1076/vesd.31.5.423.8363.
[4] Nielsen JCO, Lundén R, Johansson A, Vernersson T. Train–track interaction and mechanisms of irregular wear on wheel and rail surfaces. Vehicle Syst Dyn 2003;40:3–54. doi:10.1076/vesd.40.1.3.1587.
[5] Nielsen JCO, Oscarsson J. Simulation of dynamic train–track interaction with state-dependent track properties. J Sound Vibration 2004;275:515–32. doi:10.1016/j.jsv.2003.06.033.
[6] Zhai W, Cai Z. Dynamic interaction between a lumped mass vehicle and a discretely supported continuous rail track. Comput Struct 1997;63:987–97. doi:10.1016/S0045-7949(96)00401-4.
[7] Yau J-D, Yang Y-B, Kuo S-R. Impact response of high speed rail bridges and riding comfort of rail cars. Eng Struct 1999;21:836–44. doi:10.1016/S0141-0296(98)00037-6.
[8] Hwang ES, Nowak AS. Simulation of dynamic load for bridges. J Struct Eng 1991;117:1413–34. doi:10.1061/(ASCE)0733-9445(1991)117:5(1413).
[9] Yang FH, Fonder GA. An iterative solution method for dynamic response of bridge–vehicles systems. Earthquake Eng Struct Dyn 1996;25:195–215. doi:10.1002/(SICI)1096-9845(199602)25:2<195::AID-EQE547>3.0.CO;2-R.
[10] Delgado R, Santos SM. Modelling of railway bridge–vehicle interaction on high speed tracks. Comput Struct 1997;63:511–23. doi:10.1016/S0045-7949(96)00360-4.
[11] Yang Y-B, Yau J-D. Vehicle–bridge interaction element for dynamic analysis. J Struct Eng 1997;123:1512–8. doi:10.1061/(ASCE)0733-9445(1997)123:11(1512).
[12] Yang Y-B, Chang C-H, Yau J-D. An element for analysing vehicle–bridge systems considering vehicle's pitching effect. Int J Num Methods Eng 1999;46:1031–47. doi:10.1002/(SICI)1097-0207(19991110)46:7<1031::AID-NME738>3.0.CO;2-V.
[13] Yang Y-B, Wu Y-S. A versatile element for analyzing vehicle–bridge interaction response. Eng Struct 2001;23:452–69. doi:10.1016/S0141-0296(00)00065-1.
[14] FEMIX 4.0 – Finite Element Analysis. Available from: <http://www.alvaroazevedo.com/femix/> (Accessed 23-09-11).
[15] Hughes TJR. The finite element method: linear static and dynamic finite element analysis. New York: Dover Publications; 2000.
[16] Clough RW, Penzien J. Dynamics of structures. 2nd ed. New York: McGraw-Hill; 1993.
[17] Bathe KJ. Finite element procedures. Upper Saddle River, NJ: Prentice-Hall; 1996.
[18] Biggs JM. Introduction to structural dynamics. New York: McGraw-Hill; 1964.
[19] Benzi M, Golub GH, Liesen J. Numerical solution of saddle point problems. Acta Num 2005;14:1–137. doi:10.1017/S0962492904000212.